First U-Pb detrital zircon ages from the Los Morteritos Unit (El Gigante Metamorphic Complex), Sierras Pampeanas, Argentina: new insight into the early Paleozoic evolution of SW Gondwana

***Carlos I. Lembo Wuest[1,2], Sebastián O. Verdecchia[1,2], Juan A. Murra[1], Carlos D. Ramacciotti[1,2]**

[1] *Universidad Nacional de Córdoba. Facultad de Ciencias Exactas, Físicas y Naturales. CICTERRA (CONICET-UNC). Ingenieur Ismael Bordabehere, Av. Haya de la Torre, Córdoba, Argentina. (*E-mail: ivan.lembow@unc.edu.ar; sverdecchia@unc.edu.ar; juan.murra@unc.edu.ar; carlos.ramacciotti@unc.edu.ar)

[2] *Consejo Nacional de Investigaciones Científicas y Tecnológicas (CONICET). Centro de Investigaciones en Ciencias de la Tierra (CICTERRA). Ingenieur Ismael Bordabehere, Av. Haya de la Torre, Córdoba, Argentina.*

**Corresponding author:* ivan.lembow@unc.edu.ar

ABSTRACT. The El Gigante Metamorphic Complex, in the eponymous range (Sierras Pampeanas, Argentina), consists of three lithostratigraphic units. These are, from bottom to top: Quebrada Grande (Mesoproterozoic protoliths, predominantly igneous), Loma Cortada (Ediacaran-early Cambrian siliciclastic and carbonate protoliths), and Los Morteritos (middle to late Cambrian siliciclastic and carbonate protoliths), all reworked by the Famatinian orogeny. This study reports the first U–Pb detrital zircon age data of the Los Morteritos Unit, obtained from a quartz–micaceous schist, which shows two main Mesoproterozoic peaks (~1350 and ~1070 Ma) and minor Cambrian ages. This age pattern suggests a recycling of the underlying units and a minor contribution from the Pampean orogen**.** The graphite-rich rocks, along with an abundance of carbonate protoliths, previously published isotopic data from marbles, and the new U-Pb detrital zircon ages, support a correlation of the Los Morteritos Unit with other rocks

of the westernmost Sierras Pampeanas, such as the Caucete and Nikizanga groups in the Sierra de Pie de Palo and Cerro Pan de Azúcar. These correspond to sedimentary successions deposited in a low-energy, distal environment, belonging to a mixed carbonate–siliciclastic platform developed at the SW Gondwana margin in the middle to late Cambrian (ca. 525-490 Ma).
Keywords: Sierras Pampeanas, Mixed carbonate-siliciclastic platform, SW Gondwana, U-Pb zircon geochronology

Primeras edades U–Pb en circones detríticos de la Unidad Los Morteritos (Complejo Metamórfico El Gigante), Sierras Pampeanas, Argentina: nuevos aportes a la evolución paleozoica temprana del SO de Gondwana. El Complejo Metamórfico El Gigante, en la sierra epónima (Sierras Pampeanas, Argentina), está compuesto por tres unidades litoestratigráficas. De base a techo, estas son: Quebrada Grande (protolitos mesoproterozoicos, predominantemente ígneos), Loma Cortada (protolitos siliciclásticos y carbonáticos, ediacarianos–cámbricos tempranos) y Los Morteritos (protolitos siliciclásticos y carbonáticos, cámbricos medios a tardíos), todas ellas retrabajadas por la orogenia famatiniana. Este estudio presenta las primeras edades U–Pb en circones detríticos de la Unidad Los Morteritos, obtenidas de un esquisto cuarzoso-micáceo, que muestran dos picos principales mesoproterozoicos (~1350 y ~1070 Ma) y en menor medida edades cámbricas. Este patrón sugiere un reciclado de unidades subyacentes y una contribución menor del orógeno Pampeano. Las rocas ricas en grafito, junto con la abundancia de protolitos carbonáticos, datos isotópicos en mármoles publicados previamente, y las nuevas edades U-Pb en circones detríticos, respaldan la correlación de la Unidad Los Morteritos con otras rocas en las Sierras Pampeanas occidentales, como los Grupos Caucete y Nikizanga en la Sierra de Pie de Palo y Cerro Pan de Azúcar. Estas unidades corresponden a sucesiones sedimentarias depositadas en un ambiente distal de baja energía, pertenecientes a una plataforma mixta carbonática–siliciclástica desarrollada en el margen suroeste de Gondwana durante el Cámbrico medio a tardío (ca. 525–490 Ma).

Palabras clave: Sierras Pampeanas, Plataforma mixta carbonática-siliciclástica, SO de Gondwana, Geocronología U-Pb en circones

1. Introduction

Zircon is one of the most informative minerals in the sedimentary record, due to its exceptional resistance to surface alteration and metamorphism, as well as its ability to preserve geochemical and geochronological signatures. Thus, detrital zircon analysis has become a key tool in provenance studies and assessment of crustal evolution, particularly in ancient basins where conventional sedimentological approaches are limited by tectono-metamorphic overprinting (e.g., Fedo et al., 2003; Cawood et al., 2012).

The present-day South American continent records the amalgamation of multiple Precambrian cratonic blocks covered by Ediacaran to late Cambrian sedimentary successions (e.g., Cordani et al., 2003; Vaughan and Pankhurst, 2008; Casquet et al., 2012; Torsvik and Cocks, 2013; Ramacciotti et al., 2025). These successions, with contrasting provenance and geotectonic settings, were tectonically juxtaposed and metamorphosed during the Neoproterozoic to early Paleozoic orogenic cycles (Pampean and Famatinian orogenies) associated with the protracted assembly of SW Gondwana (e.g., Weinberg et al., 2018; Oriolo et al., 2021). In this scenario, the Sierras Pampeanas of Argentina represent a key region to assess these sedimentary successions and their tectono-metamorphic evolution, as they expose different crustal levels exhumed during the Neogene (Andean orogeny) by a flat slab subduction event (e.g., Jordan and Allmendinger, 1986; Ramos et al., 2002) (Fig. 1).

This paper focuses on the Sierra de El Gigante (SW Sierras Pampeanas) and reports the first U-Pb detrital zircon ages from the upper lithostratigraphic unit (named here Los Morteritos) of the El Gigante Metamorphic Complex, interpreted as a post-Pampean, pre-Famatinian

succession (Lembo Wuest et al., 2024; Gardini et al., 2025). To date, chronological constraints for this unit have relied solely on Sr, C, and O isotope data from marbles. The Sierra de El Gigante lies between the eastern and western Sierras Pampeanas, a region which preserves distinct geological records and has been interpreted by some authors as different terranes (e.g., Ramos et al., 1998; Fig. 1). Here, we discuss the implications of the new data and their possible regional correlations, providing new insights into the earlier stages of the SW Gondwana margin evolution.

2. Geological setting

The Sierras Pampeanas of Argentina comprise ~N-S trending mountain ranges composed mostly of igneous–metamorphic basements. Its westernmost portion is characterized by the presence of Grenvillian-aged (ca. 1330-1030 Ma) igneous–metamorphic complexes (Casquet et al., 2012; Rapela et al., 2016; Ramacciotti et al., 2022) (Fig. 1). Additionally, two ~N-S orogenic belts of Neoproterozoic to middle Paleozoic age are recognized (Fig. 1). The older, and eastern, belt corresponds to the Pampean orogen (ca. 550–515 Ma; e.g., Rapela et al., 1998; Ramos et al., 2014; Casquet et al., 2018; Zandomeni et al., 2026), whereas the younger belt is part of the Famatinian orogen and better recorded to the west (ca. 490–410 Ma; e.g., Ramos, 2018; Rapela et al., 2018; Otamendi et al., 2020; Casquet et al., 2021).

The Pampean orogeny is well-exposed in central and NW Argentina and consists of calc-alkaline arc magmatism along with low- to high-grade metamorphic rocks with anatexis and S-type granite formation (e.g., Rapela et al., 1998; von Gosen et al., 2014; Bellos et al., 2020; Tibaldi et al., 2021; Zandomeni et al., 2026). Alternative tectonic models include: the oblique subduction and subsequent collision of the Paleoproterozoic MARA (acronym of Maz, Arequipa, Río Apa; Casquet et al., 2012) block against the Kalahari craton, the collision of an

island arc attached to the Río de la Plata craton followed by the accretion of the Pampia terrane, and an initial oceanic subduction followed by the interaction of an active ridge-trench with the SW Gondwana accretionary prism (Ramos et al., 2014, and references therein).

The Famatinian orogen, on the other hand, extends from Patagonia to Venezuela and consists of I- and S-type magmatism, as well as of low- to high-grade metamorphic rocks (e.g., Ramos, 2018; Rapela et al., 2018; Otamendi et al., 2020). While its magmatic peak occurred during the Early–Middle Ordovician, its geological record comprising plutonism, volcanism, and metamorphism spans from the late Cambrian to the Devonian, with prominent exposures in the Sierras Pampeanas and the Puna plateau (e.g., Otamendi et al., 2020; Casquet et al., 2021). The Famatinian orogeny is widely interpreted as the result of the accretion of the exotic Precordillera terrane, although its Laurentian provenance and the precise timing of collision remain subjects of ongoing debate (e.g., Ramos et al., 1988; Ramacciotti et al., 2018).

The sedimentary protoliths of the metamorphic basement in the Sierras Pampeanas can be grouped, according to their provenance and relationship to the orogenic events, as follows:

1. pre-Grenvillian successions (i.e., the Maz Metasedimentary Series; Ramacciotti et al., 2022).
2. pre-Pampean successions with Laurentia-MARA provenance (i.e., the Difunta Correa Basin; Ramacciotti et al., 2025, and references therein).
3. pre- to syn-Pampean successions with Gondwanan provenance (i.e., the Puncoviscana Basin; Rapela et al., 2016, and references therein).
4. post-Pampean—pre-Famatinian successions (i.e., the Mesón Group, Nikizanga and Caucete groups and equivalents; e.g., Rapela et al., 2016; Ramacciotti et al., 2018; Franceschinis et al., 2020).

The Sierra de El Gigante, in SW Sierras Pampeanas, is primarily composed of the El Gigante Metamorphic Complex (Gardini and Dalla Salda, 1997; Fig. 2A). This complex comprises a Mesoproterozoic basement and two sedimentary covers assigned to the Difunta Correa Basin and to the post-Pampean—pre-Famatinian successions, all reworked by the Famatinian orogeny (Lembo Wuest et al., 2024; Gardini et al., 2025). It represents the most extensive geological unit of the range, which also includes subordinate Cretaceous and Cenozoic sedimentary covers exposed at its southern and northern ends (Fig. 2A).

2.1. The El Gigante Metamorphic Complex

The El Gigante Metamorphic Complex is subdivided into three lithostratigraphic units (Fig. 2B), whose original contact relationships (unconformities) have been obscured by intense deformation. The metamorphic age of this complex remains unconstrained, but it can be attributed to the Famatinian orogeny based on the age of its protoliths and tectono-metamorphic evidence nearby (Sims et al., 1998; González et al., 2004; Steenken et al., 2008). The three lithostratigraphic units are the following:

2.1.1. Quebrada Grande Unit (Mesoproterozoic protolith)

The type locality of this unit is situated in the central–eastern sector of the range (Fig. 2A). It consists of migmatites of mafic to intermediate composition, metagranitoids, and amphibolites, which mainly crop out in the south as a lens-shaped body up to ~4 km long, and also occur in other sectors as isolated bodies up to 300 m long in the hinge zones of tight folds (Figs. 2A, 3A, 3B). The migmatites (stromatites) are characterised by alternating melano- to mesosomes (amphibole, biotite, and garnet) and leucosomes (quartz and feldspars). The metagranitoids display a texture with phenocrysts (<1 cm-long plagioclase and K-feldspar) inherited from the igneous protolith, embedded in a medium- to fine-grained matrix composed mainly of quartz,

muscovite, plagioclase, K-feldspar, biotite, and occasional garnet. U-Pb zircon geochronology of the metagranitoids yielded crystallization ages of ca. 1110–1040 Ma (Lembo Wuest et al., 2024). The amphibolites occur as <10 m-thick, tabular and lenticular bodies, and have a porphyroblastic texture, with amphibole porphyroblasts within a matrix of amphibole and feldspar. This unit is overprinted, in the southern sector, by the here-defined intermediate-temperature El Monigote shear zone (Fig. 2A, C).

2.1.2. Loma Cortada Unit (Ediacaran to early Cambrian protolith)

This unit is well registered in the Quebrada Grande area (Fig. 2A). It consists of metasedimentary successions of quartzites, quartz–micaceous schists, and metacarbonates (marbles). In the central to southern sector of the range, quartzites crop out in packages up to 50 m thick, intercalated with subordinate quartz–micaceous schists and marbles less than 3 m thick (Fig. 3C, D). The relative abundance of the last two lithologies increases northward. Overall, the exposed thickness of the unit does not exceed 400 m, and in several sectors, it is bounded by thick marble layers and graphitic schists of the Los Morteritos Unit. A maximum depositional age of ca. 975 Ma, obtained from detrital zircon U-Pb analyses in quartzites, has been determined for this unit (Lembo Wuest et al., 2024). In addition, Sr isotope data from marbles indicate an Ediacaran depositional age (635–570 Ma) (Galindo et al., 2004; Rapela et al., 2007; Lembo Wuest et al., 2024). In the southern region, this unit is also affected by the El Monigote shear zone (Fig. 2A, C).

2.1.3. Los Morteritos Unit (middle to late Cambrian protolith)

This is the most extensive unit within the Sierra de El Gigante and its type locality is situated in the central–northern sector of the range along the Quebrada del Grafito (Fig. 2A). It consists of micaceous schists, quartz–micaceous schists, graphitic schists, and marbles (often graphitic;

Fig. 3E-H). Micaceous schists of this unit constitute the most abundant lithology of the range. Marbles occur as layers up to 70 m thick, commonly displaying gray, whitish, and bluish tones. Graphitic schists can reach 50 m thick in the northern sector, with colors ranging from dark gray to black. Both the marbles and the graphitic schists are useful stratigraphic markers for mapping, enabling the observation of complex folding patterns (Gardini, 1993). Quartz–micaceous schists are scarce and appear as <1 m thick intercalations. The Sr, O, and C isotope composition of marbles allowed the determination of a sedimentation age ranging from the middle to late Cambrian (Galindo et al., 2004; Lembo Wuest et al., 2024). We report here the first U-Pb detrital zircon ages from a quartz–micaceous schist of this unit.

3. Analytical methods

U-Pb zircon geochronology was performed on a quartz–micaceous schist of the Los Morteritos Unit (sample GIG 18-44) from the central-northern sector of the range (Fig. 2). The analyses were conducted at LA. TE. ANDES S.A. (GEOMAP-CONICET, Salta, Argentina) by LA-ICP-MS RESOlution-SE 193 nm combined with a triple quadrupole ICP-MS. The ages were calculated from isotopic ratios using the zircon standard 91500 as the reference material (Wiedenbeck et al., 2004), and repeated measurements of the Plešovice zircon (ID-TIMS reference age: 337.13 ± 0.37 Ma; Sláma et al., 2008) as the secondary standard. The precision of results was confirmed by obtaining the weighted mean $^{206}Pb/^{238}U$ age of the Plešovice standard. Data reduction was performed using the LADR software (v.1.1.0.6; Norris and Danyushevsky, 2018). Data processing was done using IsoplotR (Vermeesch, 2018). Common Pb was not determined. Concordia ages were used, with discordances calculated as concordia distances, rejecting analyses below -3.5 and above 4.6 (equivalent to a relative discordance of 10%; Zimmermann et al., 2018; Vermeesch, 2020). Discordant analyses are shown as open ellipses in the concordia diagrams and were excluded from age calculations and Kernel Density

Estimate plots. Tera-Wasserburg and Wetherill concordia diagrams were plotted at one sigma (1σ) error. Results are shown in figure 4 (see Supplementary Table 1 for the analytical data).

4. Results

The mineralogy of the quartz-micaceous schist analyzed in this study consists of quartz, albite, chlorite, garnet, muscovite, and biotite, with accessory apatite, epidote, zircon, iron oxides, and carbonate filling fractures (Fig. 3H). The sample has a porphyroblastic texture, with garnet poikiloblasts immersed in a medium- to fine-grained matrix mainly composed of quartz and albite. Biotite and muscovite occur sporadically, aligned with the main foliation. The garnet poikiloblasts are anhedral to subhedral and less than 1 mm in diameter. The garnet and biotite are partially replaced by chlorite.

The zircon grains range from 110 to 360 μm in length, showing subrounded to rounded shapes, although elongated euhedral crystals are also present (Fig. 4A). They often display oscillatory zoning, although some unzoned low-CL crystals also exist. Ninety spots were analysed, thirty-five of which were discarded due to high discordance (Supplementary Table 1). Excepting one spot with Th/U = 0.01, the remaining show values above 0.1, which, together with internal structures, suggest an igneous origin. The calculated ages range from 1408 to 516 Ma, with a main peak at ca. 1069 Ma and a secondary group between ca. 1382 and 1296 Ma. The youngest concordant zircon ages are 747 Ma and 516 Ma (Fig. 4C). A Cambrian zircon population includes one concordant overgrowth of 516 Ma with a slight discordant core of 533 Ma (-8.55% concordia distance; Fig. 4A), and another spot at 559 Ma (12.73% concordia distance). These zircon grains display Th/U ratios between 0.42 and 0.57, consistent with an igneous origin.

5. Discussion

5.1. Age and correlations of the sedimentary protoliths of the Los Morteritos Unit

A remarkable feature of the Los Morteritos Unit is the presence of thick layers of graphitic marbles and graphitic schists (Fig. 3E, F). This distinctive lithologic association, coupled with similar structural and metamorphic characteristics, allows for a primary correlation with other western Sierras Pampeanas successions, such as the Caucete and Nikizanga groups in the Sierra de Pie de Palo and the marbles of Cerro Pan de Azúcar (Gardini and Dalla Salda, 1997; Galindo et al., 2004; Rapela et al., 2007; Lembo Wuest et al., 2024). This correlation is supported by isotopic data: marbles from the Los Morteritos Unit yielded $^{87}Sr/^{86}Sr$ ratios of 0.7093–0.7099 and $\delta^{13}C_{PDB}$ values between –0.29 and +0.34 (Galindo et al., 2004), signatures that show a significant overlap with the isotopic ranges reported for the middle to late Cambrian Nikizanga, Caucete, and Cerro Pan de Azúcar units ($^{87}Sr/^{86}Sr$: 0.7089–0.7099 and $\delta^{13}C_{PDB}$: –0.46 to +0.02; Naipauer et al., 2005; Ramacciotti et al., 2018).

Our new U–Pb detrital zircon data further reinforce this chronostratigraphic framework. The youngest concordant age of 516 Ma (along with two slightly discordant analyses at 533 and 559 Ma) is consistent with the maximum depositional ages found in the aforementioned correlated units (Fig. 4C). Moreover, the disposition of a core at 533 Ma with an overgrowth at 516 Ma (Fig. 4A) suggests some degree of magmatic recycling (e.g., antecryst-autocryst). The Mesoproterozoic ages identified have also been reported in the Loma Cortada quartzites and the Quebrada Grande metagranitoids (Rapela et al., 2007; Lembo Wuest et al., 2024) (Fig. 4C), suggesting that these underlying units acted as primary source areas. Additionally, a concordant Neoproterozoic zircon grain yielding an age of 747 Ma was identified. Zircon grains within the ca. 850–760 Ma range are scarce in other sequences of the western Sierras Pampeanas and have been linked to A-type granitoids associated with the rifting of MARA from Laurentia (Baldo et al., 2006; Rapela et al., 2016).

5.2. Paleogeography of the SW Gondwana margin

After the Pampean orogeny and before the Famatinian orogeny, i.e., in the middle to late Cambrian (ca. 525-490 Ma), an extensive carbonate–siliciclastic platform developed along the southwestern margin of Gondwana (Collo et al., 2009; Verdecchia et al., 2014; Rapela et al., 2016; Ramacciotti et al., 2018; Hodgin et al., 2021; Tortello et al., 2026). The siliciclastic protoliths associated with this platform are characterized by the presence of detrital zircon grains with ages between 545 and 515 Ma, attributed to the Pampean orogen (see summary in Rapela et al., 2016). However, the detrital zircon age patterns vary depending on sample location. In the westernmost Sierras Pampeanas (i.e., Los Morteritos Unit, Cerro Pan de Azúcar, and Caucete Group), Mesoproterozoic ages are dominant, with minor Pampean contributions (Rapela et al., 2016; Ramacciotti et al., 2018) (Fig. 4C). An alternative interpretation suggests a Laurentian affinity for the Caucete Group, considering it part of the Cuyania terrane that accreted to SW Gondwana during the Early Ordovician (Naipauer et al., 2010); however, paleogeographic, geodynamic, and provenance considerations interpreted these rocks as derived from the reworking (cannibalization) of the underlying Difunta Correa Metasedimentary Sequence with minor contribution of the Pampean orogen (Ramacciotti et al., 2018). The easternmost Sierras Pampeanas, in contrast, which lack a record of middle to late Cambrian metacarbonate layers, display zircon populations dominated by Pampean ages (550–515 Ma), with subordinate Neoproterozoic and Mesoproterozoic contributions (Verdecchia et al., 2011; Rapela et al., 2016). The westward decrease in early Cambrian zircon ages may reflect a more distal position relative to the Pampean orogen (i.e., oceanward), as previously proposed by Ramacciotti et al. (2018). This interpretation is further supported by the increasing proportion of carbonate and organic matter content toward the west, indicative of deposition in distal, low-energy environments.

6. Conclusions

The El Gigante Metamorphic Complex consists of three lithostratigraphic units: Quebrada Grande, Loma Cortada, and Los Morteritos, with igneous and sedimentary protoliths Mesoproterozoic to late Cambrian in age, tectonically juxtaposed and metamorphosed during the Famatinian orogeny. The new U-Pb detrital zircon data from the Los Morteritos Unit indicate sedimentary recycling from the underlying Quebrada Grande and Loma Cortada units, with limited input from the Neoproterozoic-early Cambrian Pampean orogen. Regional correlations, based on lithology, isotopic signature, and geochronology, suggest that the protoliths of the Los Morteritos Unit were deposited in a low-energy distal environment of a mixed carbonate–siliciclastic platform, developed along the SW Gondwana margin during the middle to late Cambrian (ca. 525–490 Ma).

Acknowledgement

This work was funded by the projects Consolidar SECyT-UNC 2023-2028, FONCyT 2020-2891, and PIP-2015-11220150100901CO (Argentina). This article is part of the doctoral thesis of the first author, who conducted their PhD studies supported by a doctoral fellowship from CONICET. The authors are grateful to B. Hodgin, M. Naipauer, and P. Quezada for their constructive reviews, and to the editor D. Bertin for his efficient handling and support.

References

Baldo, E.G.; Casquet, C.; Pankhurst, R.J.; Galindo, C.; Rapela, C.W.; Fanning, C.M.; Dahlquist, J.; Murra, J. 2006. Neoproterozoic A-type magmatism in the Western Sierras Pampeanas (Argentina): evidence for Rodinia break-up along a proto-Iapetus rift?. Terra Nova 18: 388–394. https://doi.org/10.1111/j.1365-3121.2006.00703.x.

Bellos, L.I.; Díaz-Alvarado, J.; López, J.P.; Rodríguez, N.; Nagle, A.E.A.; Tassinari, C.C.G.; Altenberg, U.; Schleicher, A. 2020. The juxtaposition of Cambrian and early Ordovician magmatism in the Tafí del Valle area. Characteristics and recognition of Pampean and Famatinian magmatic suites in the easternmost Sierras Pampeanas. Journal of South American Earth Sciences 104: 102878. https://doi.org/10.1016/j.jsames.2020.102878

Casquet, C.; Rapela, C.W.; Pankhurst, R.J.; Baldo, E.G.; Galindo, C.; Fanning, C.M.; Dahlquist, J.A.; Saavedra, J. 2012. A history of Proterozoic terranes in southern South America: from Rodinia to Gondwana. Geoscience Frontiers 3: 137–145. https://doi.org/10.1016/j.gsf.2011.11.004

Casquet, C.; Dahlquist, J.A.; Verdecchia, S.O.; Baldo, E.G.; Galindo, C.; Rapela, C.W.; Pankhurst, R.J.; Morales Cámera, M.M.; Murra, J.A.; Fanning, C.M. 2018. Review of the Cambrian Pampean orogeny of Argentina; a displaced orogen formerly attached to the Saldania Belt of South Africa? Earth-Science Reviews 177: 209–225. https://doi.org/10.1016/j.earscirev.2017.11.013.

Casquet, C.; Alasino, P.H.; Galindo, C.; Pankhurst, R.J.; Dahlquist, J.A.; Baldo, E.G.; Ramacciotti, C.D.; Verdecchia, S.O.; Larrovere, M.A.; Rapela, C.W.; Recio, C. 2021. The Faja Eruptiva of the Eastern Puna and the Sierra de Calalaste, NW Argentina: U–Pb zircon chronology of the early Famatinian orogeny. Journal of Iberian Geology 47 (1–2): 15–37. https://doi.org/10.1007/s41513-020-00150-z.

Cawood, P.A.; Hawkesworth, C.J.; Dhuime, B. 2012. Detrital zircon record and tectonic setting. Geology 40 (10): 875–878. https://doi.org/10.1130/G32945.1

Collo, G.; Astini, R.A.; Cawood, P.A.; Buchan, C.; Pimentel, M. 2009. U–Pb detrital zircon ages and Sm–Nd isotopic features in low-grade metasedimentary rocks of the Famatina belt: implications for late Neoproterozoic–early Palaeozoic evolution of the proto-Andean margin

of Gondwana. Journal of the Geological Society 166 (2): 303–319. https://doi.org/10.1144/0016-76492008-051

Cordani, U.G.; Brito-Neves, B.B.; D'Agrella-Filho, M.S. 2003. From Rodinia to Gondwana: a review of the available evidence from South America. Gondwana Research 6 (2): 275–284. https://doi.org/10.1016/S1342-937X(05)70976-X

Fedo, C.M.; Sircombe, K.N.; Rainbird, R.H. 2003. Detrital zircon analysis of the sedimentary record. Reviews in Mineralogy and Geochemistry 53 (1): 277–303. https://doi.org/10.2113/0530277

Franceschinis, P.R.; Rapalini, A.E.; Escayola, M.P.; Piceda, C.R. 2020. Paleogeographic and tectonic evolution of the Pampia Terrane in the Cambrian: New paleomagnetic constraints. Tectonophysics 779: 228386. https://doi.org/10.1016/j.tecto.2020.228386

Galindo, C.; Casquet, C.; Rapela, C.; Pankhurst, R.; Baldo, E.; Saavedra, J. 2004. Sr, C and O isotope geochemistry and stratigraphy of Precambrian and lower Paleozoic carbonate sequences from the Western Sierras Pampeanas of Argentina: tectonic implications. Precambrian Research 131 (1–2): 55–71. https://doi.org/10.1016/j.precamres.2003.12.007

Gardini, C. 1993. La estructura íntima del basamento de la sierra de El Gigante, San Luis. Actas 12.º Congreso Geológico Argentino 3: 1–10. Mendoza.

Gardini, C.; Dalla Salda, L. 1997. El complejo metamórfico de la sierra de El Gigante, San Luis, Argentina. Revista de la Asociación Geológica Argentina 52 (2): 132–142.

Gardini, C.; Lembo Wuest, C.I.; Verdecchia, S.O.; Murra, J.A. 2025. Complejo metamórfico El Gigante. Relatorio XXII Congreso Geológico Argentino: 28–51. San Luis.

González, P.D.; Sato, A.M.; Llambias, E.J.; Basei, M.A.; Vlach, S.R. 2004. Early Paleozoic structural and metamorphic evolution of western Sierra de San Luis (Argentina), in relation to Cuyania accretion. Gondwana Research 7 (4): 1157–1170. https://doi.org/10.1016/S1342-937X(05)71091-1

Hodgin, E.B.; Gutierrez-Marco, J.C.; Colmenar, J.; Macdonald, F.A.; Carlotto, V.; Crowley, J.L.; Newmann, J.R. 2021. Cannibalization of a late Cambrian backarc in southern Peru: new insights into the assembly of southwestern Gondwana. Gondwana Research 92: 202-227. https://doi.org/10.1016/j.gr.2021.01.004

Jordan, T.E.; Allmendinger, R.W. 1986. The Sierras Pampeanas of Argentina: a modern analogue of Rocky Mountain foreland deformation. American Journal of Science 286: 737–764. https://doi.org/10.2475/ajs.286.10.737.

Lembo Wuest, C.I.; Murra, J.A.; Verdecchia, S.O.; Ramacciotti, C.D.; Baldo, E.G.; Casquet, C.; Zandomeni, P.S.; Dahlquist, J.A.; Herazo, L.; Pankhurst, R.J. 2024. The El Gigante Metamorphic Complex: A missing block with a Grenville-age basement in the Western Sierras Pampeanas, Argentina. Precambrian Research 410: 107471. https://doi.org/10.1016/j.precamres.2024.107471

Naipauer, M.; Cingolani, C.A.; Valencio, S.; Chemale, F.; Vujovich, G.I. 2005. Estudios isotópicos en carbonatos marinos del terreno Precordillera-Cuyania: ¿Plataforma común en el Neoproterozoico-Paleozoico Inferior? Latin American Journal of Sedimentology and Basin Analysis 12 (2): 89–108.

Naipauer, M.; Vujovich, G.; Cingolani, C.; McClelland, W. 2010. Detrital zircon analysis from the Neoproterozoic-Cambrian sedimentary cover (Cuyania terrane), Sierra de Pie de Palo, Argentina: evidence of a rift and passive margin system? Journal of South American Earth Sciences 29 (2): 306–326. https://doi.org/10.1016/j.jsames.2009.10.001.

Norris, A.; Danyushevsky, L. 2018. Towards Estimating the Complete Uncertainty Budget of Quantified Results Measured by LA-ICP-MS. Goldschmidt.

Oriolo, S.; Schulz, B.; Geuna, S.; González, P.D.; Otamendi, J.E.; Sláma, J.; Druguet, E.; Siegesmund, S. 2021. Early Paleozoic accretionary orogens along the Western Gondwana margin. Geoscience Frontiers 12 (1): 109–130. https://doi.org/10.1016/j. gsf.2020.07.001.

Otamendi, J.E.; Cristofolini, E.A.; Morosini, A.; Armas, P.; Tibaldi, A.M. 2020. The geodynamic history of the Famatinian arc, Argentina: a record of exposed geology over the type section (latitudes 27°–33°). Journal of South American Earth Sciences 100: 102558. https://doi.org/10.1016/j.jsames.2020.102558

Ramacciotti, C.D.; Casquet, C.; Baldo, E.G.; Galindo, C.; Pankhurst, R.; Verdecchia, S.; Rapela, C.; Fanning, M. 2018. A Cambrian mixed carbonate–siliciclastic platform in SW Gondwana: evidence from the Western Sierras Pampeanas (Argentina) and implications for the early Paleozoic paleogeography of the proto-Andean margin. International Journal of Earth Sciences 107: 2605–2625. https://doi.org/10.1007/s00531-018-1617-7

Ramacciotti, C.D.; Casquet, C.; Baldo, E.G.; Pankhurst, R.J.; Verdecchia, S.O.; Fanning, C.M.; Murra, J.A. 2022. The Maz Metasedimentary Series (Western Sierras Pampeanas, Argentina). A relict basin of the Columbia supercontinent? Geological Magazine 159 (3): 309–321. https://doi.org/10.1017/S0016756821000935

Ramacciotti, C.D.; Larrovere, M.A.; Casquet, C.; Lembo Wuest, C.I.; Morales Cámera, M.; Alasino, P.H.; Murra, J.A.; Riveros, A.; Basei, M.A.S.; Herazo, L.; Baldo, E.G. 2025. The Ediacaran margin of the Proterozoic MARA block and the sedimentary basins of the Clymene Ocean: Insights from U–Pb zircon geochronology in the Puna-Sierras Pampeanas transition, NW Argentina. Precambrian Research 422: 107792. https://doi.org/10.1016/j.precamres.2025.107792

Ramos, V.A. 2018. The Famatinian Orogen Along the Protomargin of Western Gondwana: Evidence for a Nearly Continuous Ordovician Magmatic Arc Between Venezuela and Argentina. In The Evolution of the Chilean-Argentinean Andes. Springer Earth System Sciences: 133–161. https://doi.org/10.1007/978-3-319-67774-3_6

Ramos, V.A. 1988. Late Proterozoic-early Paleozoic of the South America: a collisional history. Episodes 11: 168–174. https://doi.org/10.18814/epiiugs/1988/v11i3/003.

Ramos, V.A.; Dallmeyer, R.D.; Vujovich, G. 1998. Time constraints on the Early Palaeozoic docking of the Precordillera, central Argentina. Geological Society, London, Special Publications 142 (1): 143–158. https://doi.org/10.1144/GSL.SP.1998.142.01.08

Ramos, V.A.; Cristallini, E.O.; Pérez, D.J. 2002. The Pampean flat-slab of the Central Andes. Journal of South American Earth Sciences 15 (1): 59–78. https://doi.org/10.1016/S0895-9811(02)00006-8

Ramos, V.A.; Martino, R.D.; Otamendi, J.E.; Escayola, M.P. 2014. Evolución geotectónica de las Sierras Pampeanas Orientales. En Geología y Recursos Minerales de la Provincia de Córdoba, Relatorio del XIX Congreso Geológico Argentino (Martino, R.D.; Guereschi, A.B.; editores): 965–977.

Rapela, C.W.; Pankhurst, R.J.; Casquet, C.; Baldo, E.G.; Saavedra, J.; Galindo, C. 1998. Early evolution of the Proto-Andean margin of South America. Geology 26: 707–710.https://doi.org/10.1130/0091-7613(1998)026%3C0707:EEOTPA%3E2.3.CO;2

Rapela, C.W.; Pankhurst, R.J.; Casquet, C.; Fanning, C.M.; Baldo, E.G.; González-Casado, J.M.; Galindo, C.; Dahlquist, J.A. 2007. The Río de la Plata craton and the assembly of SW Gondwana. Earth-Science Reviews 83: 49–82. https://doi.org/10.1016/j.earscirev.2007.03.004

Rapela, C.W.; Verdecchia, S.O.; Casquet, C.; Pankhurst, R.J.; Baldo, E.G.; Galindo, C.; Murra, J.A.; Dahlquist, J.A.; Fanning, C.M. 2016. Identifying Laurentian and SW Gondwana sources in the Neoproterozoic to early Paleozoic metasedimentary rocks of the Sierras Pampeanas: Paleogeographic and tectonic implications. Gondwana Research 32: 193–212. https://doi.org/10.1016/j.gr.2015.02.010

Rapela, C.W.; Pankhurst, R.J.; Casquet, C.; Dahlquist, J.A.; Fanning, C.M.; Baldo, E.G.; Galindo, C.; Alasino, P.; Ramacciotti, C.; Verdecchia, S.O.; Murra, J.A.; Basei, M. 2018. A review of the Ordovician Famatinian orogeny in southern South America: evidence of

lithosphere reworking and continental subduction in the early proto-Andean margin of Gondwana. Earth-Science Reviews 187: 259–285. https://doi.org/10.1016/j.earscirev.2018.10.006

Sims, J.; Ireland, T.; Camacho, A.; Lyons, P.; Pieters, P.; Skirrow, R.; Stuart-Smith, P.; Miró, R. 1998. U–Pb, Th–Pb and Ar–Ar geochronology from the southern Sierras Pampeanas, Argentina: implications for the Paleozoic tectonic evolution of the western Gondwana margin. In Proto-Andean margin of Gondwana (Pankhurst, R.; Rapela, C.; editores). Geological Society of London, Special Publication 142: 259–281.. https://doi.org/10.1144/GSL.SP.1998.142.01.13

Sláma, J.; Košler, J.; Condon, D.J.; Crowley, J.L.; Gerdes, A.; Hanchar, J.M.; Horstwood, M.S.A.; Morris, G.A.; Nasdala, L.; Norberg, N.; Schaltegger, U.; Schoene, B.; Tubrett, M.N.; Whitehouse, M.J. 2008. Plešovice zircon — A new natural reference material for U–Pb and Hf isotopic microanalysis. Chemical Geology 249: 1–35. https://doi.org/10.1016/j.chemgeo.2007.11.005.

Steenken, A.; Siegesmund, S.; Wemmer, K.; de Luchi, M.G.L. 2008. Time constraints on the Famatinian and Achalian structural evolution of the basement of the Sierra de San Luis (Eastern Sierras Pampeanas, Argentina). Journal of South American Earth Sciences 25 (3): 336–358. https://doi.org/10.1016/j.jsames.2007.05.002

Tibaldi, A.M.; Otamendi, J.E.; Demichelis, A.H.; Barzola, M.G.; Barra, F.; Rabbia, O.M.; Cristofolini, E.A.; Benito, M.P. 2021. Early Cambrian multiple-sourced plutonism in the Eastern Sierras Pampeanas, Córdoba, Argentina: Implications for the evolution of the early Paleozoic Gondwana margin. Journal of South American Earth Sciences 106: 103048. https://doi.org/10.1016/j.jsames.2020.103048

Torsvik, T.H.; Cocks, L.R.M. 2013. Gondwana from top to base in space and time. Gondwana Research 24: 999–1030. https://doi.org/10.1016/j.gr.2013.06.012.

Tortello, F.; Hodgin, E.B.; Rábano, I.; Gutiérrez-Marco, J.C. 2026. Late Cambrian and Early Ordovician trilobites from the Peruvian Altiplano and their significance to the Central Andean region of South America. Journal of Paleontology, 1-17. doi:10.1017/jpa.2025.10205

Vaughan, A.P.M.; Pankhurst, R.J. 2008. Tectonic overview of the West Gondwana margin. Gondwana Research 13: 150–162. https://doi.org/10.1016/j.gr.2007.07.004

Verdecchia, S.O.; Casquet, C.; Baldo, E.G.; Rapela, C.W.; Pankhurst, R.J.; Fanning, M.; Galindo, C. 2011. Mid to Late Cambrian docking of the Río de la Plata craton to southwestern Gondwana: age constraints from U–Pb SHRIMP detrital zircon ages from Sierras de Ambato and Velasco (Sierras Pampeanas, Argentina). Journal of the Geological Society 168: 1061–1071. http://dx.doi.org/10.1144/0016-76492010-143

Verdecchia, S.O.; Murra, J.A.; Baldo, E.G.; Casquet, C.; Pascua, I.; Saavedra, J. 2014. Geoquímica de las rocas metasedimentarias del Cámbrico medio al Ordovícico temprano de la Sierra de Los Llanos (Sierras Pampeanas, Argentina): Fuente de sedimentos, correlación y ambiente geotectónico. Andean Geology 41 (2): 380–400. http://dx.doi.org/10.5027/andgeoV41n2-a06

Verdecchia, S.O.; Casquet, C.; Baldo, E.G.; Larrovere, M.A.; Lembo Wuest, C.I.; Benítez, M.E.; Ramacciotti, C.D.; Murra, J.A.; Pankhurst, R.J. 2023. Silurian inverted Barrovian-type metamorphism in the Western Sierras Pampeanas (Argentina): a case of top to bottom heating? Geological Magazine 160 (5): 972–992. https://doi.org/10.1017/S0016756823000080

Vermeesch, P. 2018. IsoplotR: A free and open toolbox for geochronology. Geoscience Frontiers 9 (5): 1479–1493. https://doi.org/10.1016/j.gsf.2018.04.001

Vermeesch, P. 2020. On the treatment of discordant detrital zircon U–Pb data. Geochronology Discussions 2020: 1–19. https://doi.org/10.5194/gchron-3-247-2021

von Gosen, W.; McClelland, W.C.; Loske, W.; Martínez, J.C.; Prozzi, C. 2014. Geochronology of igneous rocks in the Sierra Norte de Córdoba (Argentina): Implications for the Pampean evolution at the western Gondwana margin. Lithosphere 6 (4): 277–300. https://doi.org/10.1130/L344.1.

Weinberg, R.F.; Becchio, R.; Farias, P.; Suzaño, N.; Sola, A. 2018. Early Paleozoic accretionary orogenies in NW Argentina: Growth of West Gondwana. Earth-Science Reviews 187: 219–247. https://doi.org/10.1016/j.earscirev.2018.10.001

Wiedenbeck, M.; Hanchar, J.M.; Peck, W.H.; Sylvester, P.; Valley, J.; Whitehouse, M.; Kronz, A.; Morishita, Y.; Nasdala, L.; Fiebig, J.; Franchi, I.; Girard, J.P.; Greenwood, R.C.; Hinton, R.; Kita, N.; Mason, P.R.D.; Norman, M.; Ogasawara, M.; Piccoli, P.M.; Rhede, D.; Satoh, H.; Schulz-Dobrick, B.; Skår, O.; Spicuzza, M.; Terada, K.; Tindle, A.; Togashi, S.; Vennemann, T.; Xie, Q.; Zheng, Y.F. 2004. Further Characterisation of the 91500 Zircon Crystal. Geostandards and Geoanalytical Research 28: 9–39. https://doi.org/10.1111/j.1751-908X.2004.tb01041.x

Zandomeni, P.S.; Moreno, J.A.; Morales Cámera M.M.; Verdecchia, S.O.; Baldo, E.G.; Dahlquist, J.A.; Casquet, C.; Basei, M.A.S.; Santos da Cruz, G.; Rapela, C.W. 2026. The late Ediacaran to early Cambrian subduction-related granitic magmatism of the Pampean orogen: Geochemical and isotopic constraints on hybridization processes. Gondwana Research 150: 228–253. https://doi.org/10.1016/j.gr.2025.09.012

Zimmermann, S.; Mark, C.; Chew, D.; Voice, P.J. 2018. Maximising data and precision from detrital zircon U-Pb analysis by LA-ICPMS: The use of core-rim ages and the single-analysis concordia age. Sedimentary Geology 375: 5–13. https://doi.org/10.1016/j.sedgeo.2017.12.020

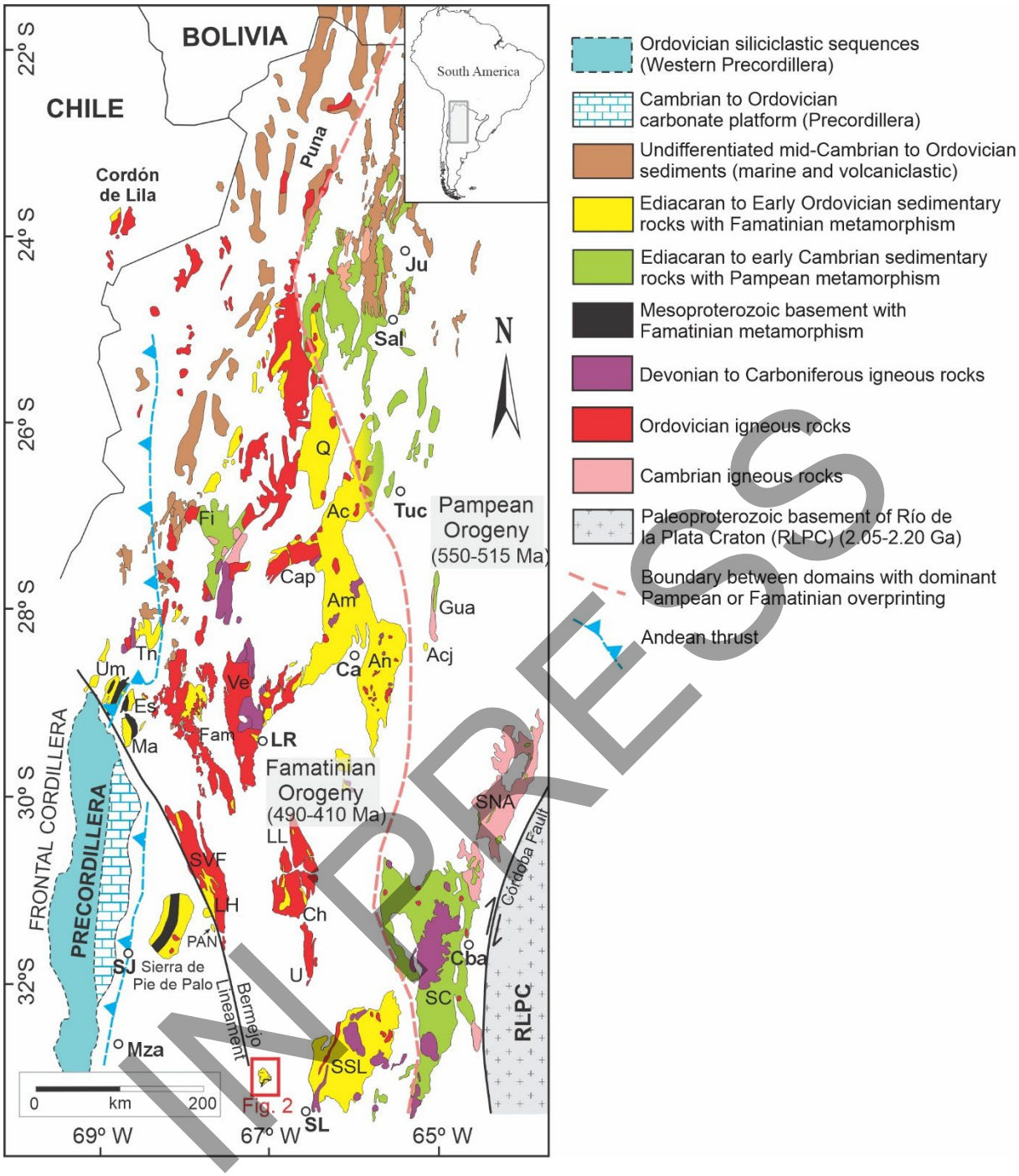

Fig. 1. Regional geological map of central and northwestern Argentina, modified after Verdecchia et al. (2023). White circles refer to cities: Jujuy (Ju), Salta (Sal), Tucumán (Tuc), Catamarca (Ca), La Rioja (LR), San Juan (SJ), Córdoba (Cba), San Luis (SL), and Mendoza (Mza). Loose text indicates ranges and other geological sites of interest: Quilmes (Q), Aconquija (Ac), Capillitas (Cap), Fiambalá (Fi), Toro Negro (Tn), Umango (Um), Espinal (Es), Maz (Ma), Famatina (Fam), Velasco (Ve), Ampato (Am), Ancasti (An), Ancaján (Acj),

Guasayán (Gua), Norte-Ambargasta (SNA), Córdoba (SC), San Luis (SSL), Ulapes (U), Chepes (Ch), Los Llanos (LL), La Huerta (LH), Valle Fertíl (SVF), and Cerro Pan de Azúcar (PAN). The location of the Sierra de El Gigante is shown at the bottom and in figure 2.

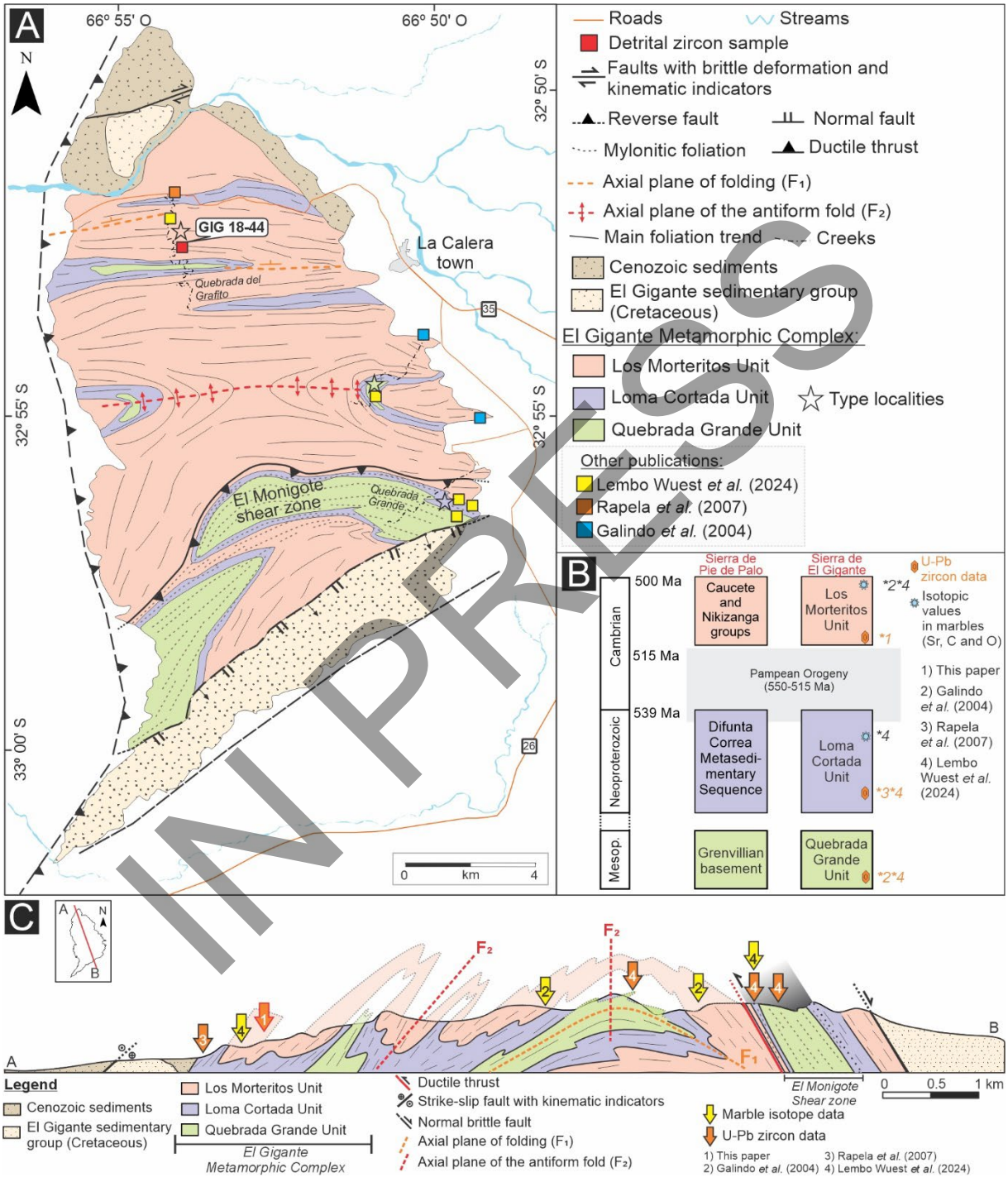

Fig. 2. A. Geological map with lithostratigraphic units of the Sierra de El Gigante (modified from Lembo Wuest et al., 2024), showing the location of the analyzed sample GIG 18-44. (See figure 1 for location.) **B.** Stratigraphic relationships of the units of the El Gigante Metamorphic

Complex and correlation with units of the Sierra de Pie de Palo. **C.** Schematic NNW-SSE geological section with simplified units (after Lembo Wuest et al., 2024).

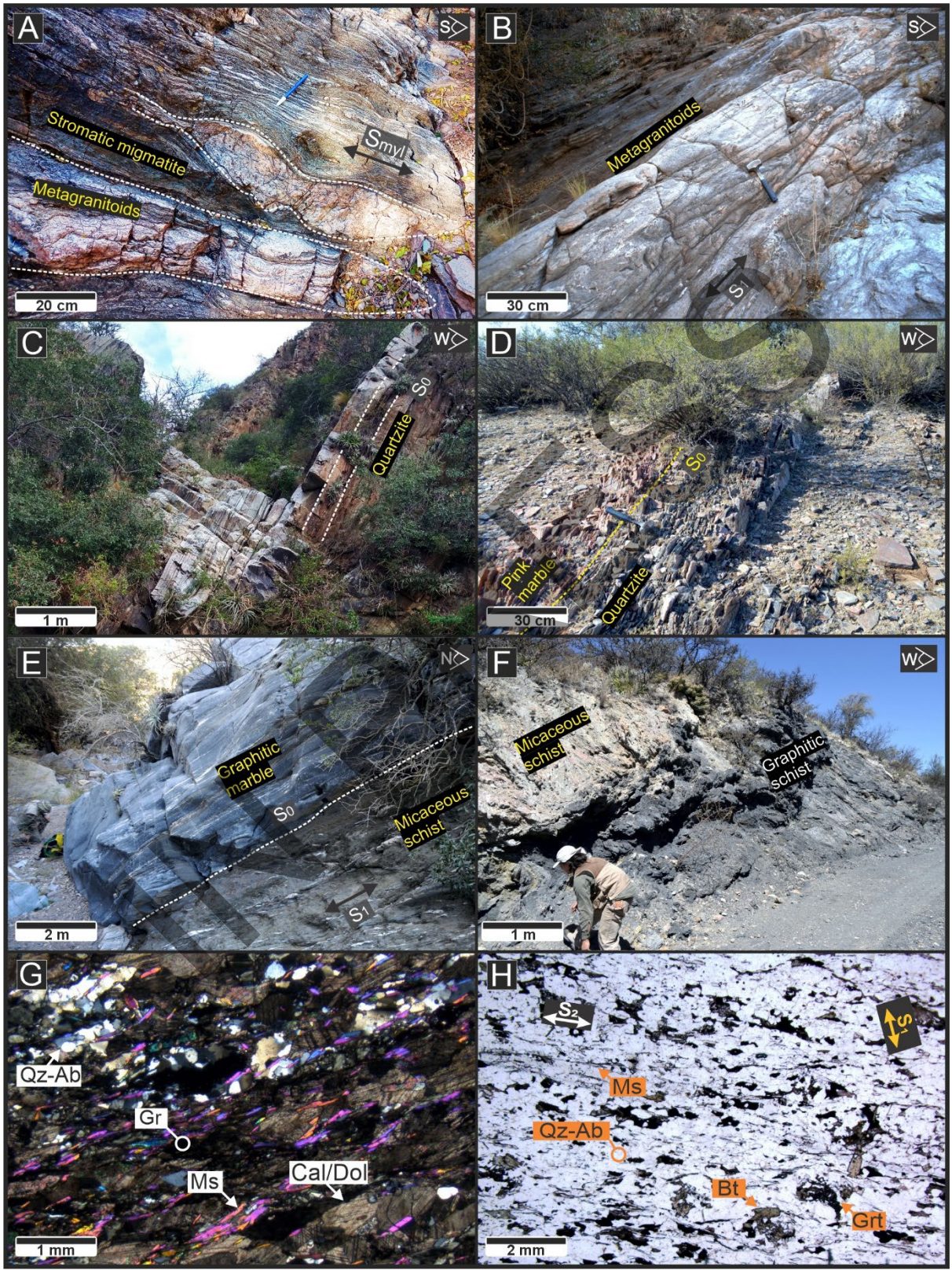

Fig. 3. Field and petrographic characteristics of the El Gigante Metamorphic Complex. **A.** Stromatic migmatite from the southern sector with lenses of metagranitoids (Quebrada Grande Unit). **B.** Layers of metagranitoids in the central-eastern area within the type locality of the Quebrada Grande Unit. **C.** Thick tabular body of whitish quartzites in the southeastern sector (Loma Cortada Unit). **D.** Intercalation of quartzites and pink marble packages in the southeastern sector, corresponding to the type locality of the Loma Cortada Unit. **E.** Contact between graphitic marbles and micaceous schists in the central-northern part of the range, corresponding to the type locality of the Los Morteritos Unit. **F.** Graphitic schists with intercalations of micaceous schists along the northern road of the sierra (Los Morteritos Unit). **G.** Photomicrograph of a graphitic marble with abundant accessory mineral phases including quartz, albite, and muscovite (cross-polarized light; Los Morteritos Unit). **H.** Photomicrograph of the quartz–micaceous schist sampled for U–Pb zircon geochronology (GIG 18-44 sample) (parallel-polarized light; Los Morteritos Unit). Ab: albite, Bt: biotite, Cal: calcite, Dol: dolomite, Gr: graphite, Grt: garnet, Ms: muscovite, Qz: quartz.

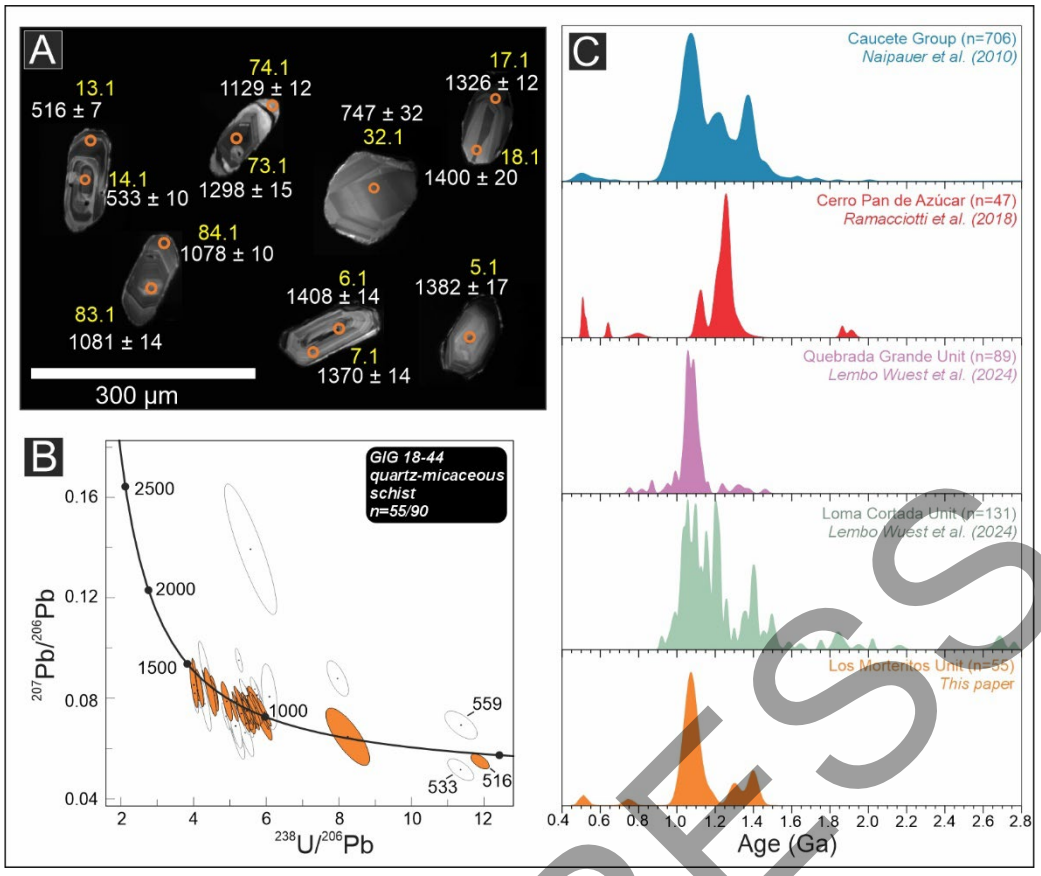

Fig. 4. A. Cathodoluminescence images of zircon grains (yellow = grain-spot number; white = age ± 1σ). **B.** Tera-Wasserburg diagram. Open ellipses correspond to discarded data due to high discordance (see text). Concordia ages (Ma) of the youngest zircon grains are indicated. **C.** Kernel Density Estimation diagrams of detrital zircon grains from the Los Morteritos Unit (Sierra de El Gigante; this paper), Loma Cortada Unit (Sierra de El Gigante; Lembo Wuest et al., 2024), Quebrada Grande Unit (Sierra de El Gigante; Lembo Wuest et al., 2024), Cerro Pan de Azúcar (Ramacciotti et al., 2018), and Caucete Group (Sierra de Pie de Palo; Naipauer et al., 2010). Concordia ages were used in the present publication; n = number of analyses.

Supplementary Table 1. U, Th, Pb isotopic ratios and U-Pb detrital zircon ages, Los Morteritos Unit, El Gigante Metamorphic Complex (Sierras Pampeanas, Argentina).

	Chemical contents (ppm)			Radiogenic ratios								Ages (Ma)								
Grain-spot	Th	U	Th/U	$^{207}Pb/^{235}U$	1σ	$^{206}Pb/^{238}U$	1σ	$^{207}Pb/^{206}Pb$	1σ	Rho XY	Rho YZ	$^{207}Pb/^{235}U$	1σ	$^{206}Pb/^{238}U$	1σ	$^{207}Pb/^{206}Pb$	1σ	Concordia age	1σ	Concordia distance
1.1	44.09	122.24	0.36	1.9686	0.0880	0.2026	0.0025	0.0818	0.0023	**0.0283**	**1.0644**	1104.84	30.11	1189.26	13.36	1239.75	56.10	**1174.68**	12.15	3.39
2.1	72.90	277.11	0.26	1.5804	0.0714	0.1709	0.0023	0.0737	0.0023	**0.0325**	**1.0008**	962.53	28.11	1017.14	12.79	1031.33	63.67	**1007.67**	11.66	1.54
3.1	48.47	102.91	0.47	1.5174	0.0709	0.1784	0.0025	0.0746	0.0023	**0.0358**	**1.0952**	937.42	28.58	1058.05	13.88	1056.04	62.57	**1033.15**	12.36	-2.69
4.1	34.65	78.27	0.44	1.5267	0.0771	0.1756	0.0027	0.0719	0.0025	**0.0346**	**1.0808**	941.18	30.98	1043.03	14.61	982.89	69.78	**1023.35**	13.12	-1.66
5.1	28.95	64.59	0.45	2.5502	0.1328	0.2443	0.0037	0.0854	0.0032	**0.0278**	**1.1508**	1286.51	37.99	1409.10	19.14	1322.92	72.85	**1381.99**	16.84	-2.23
6.1	84.00	150.10	0.56	2.7302	0.1312	0.2469	0.0030	0.0905	0.0021	**0.0231**	**1.4279**	1336.72	35.70	1422.63	15.67	1435.47	44.73	**1407.93**	14.25	1.84
7.1	77.24	108.66	0.71	2.4818	0.1059	0.2425	0.0030	0.0856	0.0023	**0.0280**	**1.3047**	1266.75	30.88	1399.42	15.37	1328.38	51.33	**1370.38**	13.53	-1.84
8.1	12.63	19.82	0.64	1.4170	0.1334	0.1744	0.0050	0.0765	0.0049	**0.0376**	**1.0282**	896.11	56.06	1036.48	27.53	1106.53	127.49	**1006.45**	24.36	5.81
9.1	36.97	74.73	0.49	1.7226	0.0937	0.1792	0.0029	0.0805	0.0029	**0.0312**	**1.0108**	1017.00	34.95	1062.75	15.97	1208.55	70.69	**1054.82**	14.57	6.66
10.1	68.94	105.02	0.66	1.7233	0.0830	0.1791	0.0033	0.0737	0.0027	**0.0392**	**1.2192**	1017.27	30.95	1062.21	17.78	1032.38	73.16	**1050.99**	15.51	-0.86
11.1	104.92	285.97	0.37	1.6106	0.0509	0.1821	0.0018	0.0722	0.0016	**0.0356**	**1.1066**	974.35	19.78	1078.70	9.87	991.76	46.04	**1056.56**	8.76	-2.33
12.1	46.90	83.34	0.56	1.6499	0.0870	0.1753	0.0027	0.0763	0.0027	**0.0315**	**1.0228**	989.50	33.33	1041.03	15.05	1101.54	70.33	**1032.23**	13.75	3.26
13.1	95.24	220.82	0.43	0.6107	0.0265	0.0843	0.0012	0.0551	0.0020	**0.0444**	**0.6010**	483.98	16.71	521.57	7.00	414.50	79.49	**516.15**	6.52	-3.39
14.1	64.66	113.06	0.57	0.5711	0.0414	0.0882	0.0018	0.0518	0.0028	**0.0440**	**0.6413**	458.74	26.76	544.95	10.79	276.03	125.55	**532.63**	10.02	-8.55
15.1	38.67	100.70	0.38	1.7628	0.0885	0.1737	0.0030	0.0815	0.0039	**0.0339**	**0.7777**	1031.88	32.54	1032.34	16.46	1232.50	92.78	**1032.25**	14.88	8.22
16.1	67.32	197.63	0.34	1.7348	0.0661	0.1828	0.0021	0.0754	0.0019	**0.0312**	**1.0683**	1021.52	24.54	1082.07	11.24	1077.49	51.41	**1071.36**	10.22	-1.03
17.1	78.52	184.38	0.43	2.5253	0.0955	0.2305	0.0026	0.0874	0.0026	**0.0270**	**1.0084**	1279.36	27.51	1337.04	13.53	1368.13	56.41	**1325.53**	12.13	2.30
18.1	58.54	103.19	0.57	2.7052	0.1412	0.2481	0.0046	0.0855	0.0026	**0.0326**	**1.7457**	1329.87	38.69	1428.80	23.76	1325.95	59.68	**1400.07**	20.03	-2.74
19.1	32.02	132.58	0.24	1.9068	0.0970	0.1930	0.0026	0.0787	0.0024	**0.0265**	**1.0507**	1083.46	33.89	1137.87	13.90	1163.94	61.64	**1129.91**	12.87	1.80
20.1	1.75	205.41	0.01	1.6295	0.0581	0.1815	0.0020	0.0732	0.0018	**0.0345**	**1.0859**	981.68	22.44	1075.01	10.94	1018.62	51.06	**1056.14**	9.78	-1.54
21.1	48.74	108.19	0.45	1.7153	0.0796	0.1803	0.0038	0.0734	0.0023	**0.0473**	**1.6173**	1014.27	29.78	1068.77	20.55	1023.49	64.17	**1050.90**	17.02	-1.34
22.1	6.33	21.80	0.29	1.8456	0.1856	0.1890	0.0050	0.0729	0.0044	**0.0269**	**1.1448**	1061.87	66.22	1115.76	27.04	1009.87	121.20	**1107.94**	25.05	-3.71
23.1	22.90	44.57	0.51	1.6299	0.1623	0.1714	0.0065	0.0743	0.0059	**0.0401**	**1.1105**	981.81	62.66	1019.62	35.80	1048.51	158.96	**1010.33**	31.33	2.07
24.1	15.12	32.62	0.46	1.7696	0.1293	0.1812	0.0039	0.0763	0.0037	**0.0304**	**1.0619**	1034.37	47.41	1073.38	21.42	1102.97	96.83	**1066.78**	19.61	1.81

25.1	23.71	39.54	0.60	1.8284	0.1518	0.1761	0.0040	0.0779	0.0040	**0.0267**	**1.0138**	1055.72	54.50	1045.88	22.18	1144.17	101.79	**1047.20**	20.76	3.90
26.1	21.53	63.19	0.34	1.8138	0.1363	0.1943	0.0047	0.0666	0.0041	**0.0346**	**1.1583**	1050.44	49.18	1144.85	25.42	823.63	127.49	**1123.84**	22.43	-11.29
27.1	62.84	158.56	0.40	1.8287	0.0762	0.1759	0.0022	0.0729	0.0022	**0.0286**	**0.9748**	1055.83	27.36	1044.55	11.94	1010.52	62.16	**1046.25**	11.08	-1.52
28.1	33.97	87.28	0.39	1.9996	0.1018	0.1749	0.0035	0.0763	0.0026	**0.0341**	**1.3274**	1115.38	34.45	1038.96	19.06	1101.11	68.64	**1054.99**	17.20	1.68
29.1	19.96	54.85	0.36	1.9405	0.1264	0.1859	0.0032	0.0740	0.0029	**0.0252**	**1.1080**	1095.18	43.65	1099.24	17.35	1039.71	78.62	**1098.71**	16.25	-2.38
30.1	23.30	56.05	0.42	1.9606	0.1140	0.1870	0.0039	0.0764	0.0029	**0.0342**	**1.3252**	1102.07	39.09	1105.26	21.20	1105.63	77.02	**1104.56**	18.88	0.09
31.1	65.18	97.90	0.67	1.6969	0.0938	0.1770	0.0029	0.0748	0.0025	**0.0308**	**1.1372**	1007.38	35.31	1050.40	15.81	1061.31	68.30	**1043.21**	14.48	1.16
32.1	10.84	17.57	0.62	1.2490	0.2005	0.1213	0.0058	0.0649	0.0075	**0.0290**	**0.7732**	822.97	90.51	738.11	33.40	771.31	243.58	**746.68**	31.95	0.98
33.1	67.48	191.15	0.35	1.9292	0.0697	0.1810	0.0026	0.0731	0.0020	**0.0371**	**1.3014**	1091.25	24.17	1072.70	14.12	1016.13	55.09	**1077.19**	12.44	-2.68
34.1	7.78	19.56	0.40	2.5886	0.5315	0.2298	0.0068	0.0911	0.0056	**0.0128**	**1.2207**	1297.42	150.39	1333.38	35.57	1448.15	116.14	**1331.47**	34.63	5.03
35.1	13.90	39.87	0.35	1.9250	0.1370	0.1763	0.0038	0.0753	0.0036	**0.0279**	**1.0664**	1089.79	47.57	1046.68	20.97	1076.92	95.57	**1053.06**	19.52	0.84
36.1	28.74	47.36	0.61	1.6562	0.1469	0.1255	0.0031	0.0881	0.0046	**0.0209**	**0.6616**	991.92	56.14	762.23	17.57	1384.00	101.07	**776.37**	17.18	23.97
37.1	13.78	19.54	0.71	1.8049	0.1744	0.1708	0.0050	0.0790	0.0052	**0.0289**	**0.9802**	1047.22	63.15	1016.74	27.80	1170.44	129.14	**1021.30**	25.84	5.90
38.1	59.64	116.28	0.51	1.9002	0.1327	0.1710	0.0045	0.0748	0.0045	**0.0336**	**0.9851**	1081.16	46.44	1017.42	24.57	1061.10	121.92	**1029.98**	22.30	1.18
39.1	7.82	20.16	0.39	2.5159	0.2348	0.2309	0.0060	0.0780	0.0044	**0.0256**	**1.3569**	1276.64	67.82	1339.14	31.52	1147.06	112.92	**1327.70**	28.53	-7.17
40.1	77.25	211.05	0.37	2.1973	0.0982	0.1755	0.0026	0.0838	0.0032	**0.0260**	**0.8068**	1180.18	31.18	1042.35	14.02	1287.97	73.58	**1061.32**	13.20	8.67
41.1	73.38	114.87	0.64	1.9442	0.1306	0.1858	0.0043	0.0708	0.0032	**0.0328**	**1.3413**	1096.46	45.05	1098.54	23.29	949.75	92.36	**1098.12**	20.95	-5.97
42.1	76.83	149.66	0.51	2.0419	0.0839	0.1845	0.0025	0.0738	0.0021	**0.0301**	**1.2153**	1129.59	28.00	1091.71	13.73	1034.21	56.87	**1098.49**	12.57	-2.92
43.1	115.67	208.56	0.55	1.9729	0.0782	0.1805	0.0020	0.0757	0.0019	**0.0258**	**1.0446**	1106.29	26.70	1069.85	11.02	1085.01	51.21	**1074.70**	10.34	0.41
44.1	108.32	291.21	0.37	1.9484	0.0628	0.1776	0.0018	0.0748	0.0017	**0.0289**	**1.0505**	1097.90	21.61	1053.61	9.93	1062.86	46.42	**1060.65**	9.19	0.55
45.1	57.10	103.68	0.55	1.9169	0.2057	0.1640	0.0039	0.0808	0.0086	**0.0190**	**0.4520**	1086.99	71.60	978.83	21.60	1216.32	209.93	**986.21**	20.98	9.08
46.1	83.48	192.69	0.43	3.0611	0.1083	0.2377	0.0026	0.0853	0.0020	**0.0241**	**1.3271**	1423.00	27.09	1374.51	13.61	1321.75	44.72	**1383.53**	12.39	-2.96
47.1	90.71	148.15	0.61	2.5990	0.1489	0.1900	0.0024	0.0953	0.0031	**0.0158**	**0.7500**	1300.36	42.01	1121.52	12.77	1533.83	62.06	**1132.89**	12.45	16.49
48.1	87.49	163.27	0.54	3.7072	0.5941	0.1791	0.0151	0.1395	0.0126	**0.0254**	**1.1926**	1572.93	128.16	1062.17	82.48	2220.56	157.11	**1150.03**	78.38	44.21
49.1	45.66	134.08	0.34	1.8753	0.0821	0.1820	0.0036	0.0746	0.0023	**0.0436**	**1.5881**	1072.40	29.00	1078.16	19.54	1056.49	60.90	**1076.40**	16.50	-0.75
50.1	30.18	75.53	0.40	1.9980	0.1076	0.1861	0.0042	0.0722	0.0028	**0.0389**	**1.4814**	1114.85	36.45	1100.16	22.75	991.56	79.54	**1104.10**	19.70	-4.73
51.1	112.08	142.64	0.79	2.6871	0.1472	0.2359	0.0029	0.0829	0.0022	**0.0197**	**1.3471**	1324.92	40.54	1365.42	15.14	1266.70	50.74	**1360.42**	14.20	-3.79
52.1	60.18	189.91	0.32	2.9914	0.1028	0.2403	0.0027	0.0857	0.0019	**0.0258**	**1.3741**	1405.43	26.14	1388.04	13.80	1330.33	43.64	**1391.66**	12.38	-2.73
53.1	60.64	105.16	0.58	2.5675	0.1111	0.2179	0.0035	0.0826	0.0023	**0.0311**	**1.5315**	1291.43	31.62	1270.72	18.27	1260.08	53.28	**1275.66**	16.10	-0.88
54.1	53.47	67.34	0.79	2.0789	0.1159	0.1900	0.0031	0.0799	0.0029	**0.0272**	**1.0911**	1141.89	38.21	1121.46	17.06	1194.36	71.25	**1124.64**	15.79	2.75

55.1	52.46	49.93	1.05	1.8761	0.1211	0.1822	0.0040	0.0716	0.0031	**0.0327**	**1.2877**	1072.67	42.76	1078.76	21.58	974.64	87.48	**1077.56**	19.49	-4.11
56.1	38.98	82.68	0.47	1.9785	0.1026	0.1827	0.0032	0.0768	0.0027	**0.0309**	**1.1933**	1108.21	34.98	1081.83	17.28	1114.70	69.08	**1086.66**	15.76	1.01
57.1	105.61	263.40	0.40	1.9093	0.0641	0.1871	0.0019	0.0730	0.0017	**0.0302**	**1.1306**	1084.35	22.38	1105.66	10.52	1012.42	47.61	**1101.88**	9.59	-3.49
58.1	21.21	39.80	0.53	1.8951	0.1303	0.1831	0.0041	0.0811	0.0037	**0.0315**	**1.1100**	1079.39	45.70	1083.71	22.39	1223.89	89.61	**1082.90**	20.33	5.83
59.1	34.78	82.99	0.42	0.8875	0.0547	0.0881	0.0023	0.0696	0.0037	**0.0417**	**0.6226**	645.01	29.42	544.47	13.52	914.39	108.44	**559.09**	12.68	12.73
60.1	172.24	205.91	0.84	2.5697	0.1146	0.2180	0.0034	0.0813	0.0025	**0.0298**	**1.3498**	1292.07	32.60	1271.14	18.06	1228.06	61.04	**1275.82**	16.07	-2.18
61.1	53.33	118.37	0.45	1.7390	0.0772	0.1842	0.0025	0.0729	0.0022	**0.0320**	**1.1086**	1023.11	28.61	1089.67	13.43	1011.31	61.87	**1077.33**	12.15	-2.34
62.1	83.11	216.42	0.38	1.8012	0.0661	0.1843	0.0021	0.0708	0.0018	**0.0319**	**1.1872**	1045.91	23.95	1090.55	11.49	949.70	51.42	**1082.16**	10.40	-5.03
63.1	47.22	75.22	0.63	1.6495	0.0853	0.1840	0.0029	0.0716	0.0025	**0.0335**	**1.1284**	989.37	32.68	1088.93	15.57	972.92	72.21	**1069.38**	13.96	-3.39
64.1	67.78	149.88	0.45	1.7613	0.0725	0.1925	0.0023	0.0684	0.0019	**0.0323**	**1.2112**	1031.32	26.66	1134.70	12.67	881.24	58.49	**1114.37**	11.35	-8.68
65.1	26.98	22.70	1.19	1.6394	0.1538	0.1841	0.0054	0.0665	0.0042	**0.0348**	**1.2701**	985.47	59.17	1089.27	29.17	821.57	132.42	**1067.67**	25.96	-9.05
66.1	68.77	113.07	0.61	1.7690	0.0790	0.1927	0.0025	0.0700	0.0021	**0.0322**	**1.1972**	1034.16	28.95	1136.18	13.76	927.17	62.39	**1116.16**	12.33	-6.97
67.1	45.36	107.80	0.42	1.8487	0.0934	0.2037	0.0030	0.0730	0.0024	**0.0323**	**1.2689**	1062.96	33.30	1195.24	16.17	1014.21	66.03	**1167.52**	14.34	-5.51
68.1	168.40	247.10	0.68	1.8338	0.0785	0.1991	0.0035	0.0730	0.0019	**0.0451**	**1.8652**	1057.65	28.12	1170.52	19.04	1012.72	52.73	**1132.82**	15.59	-4.26
69.1	84.85	186.86	0.45	1.8227	0.0688	0.1889	0.0022	0.0737	0.0021	**0.0316**	**1.0453**	1053.66	24.75	1115.34	11.78	1033.00	56.95	**1103.69**	10.63	-2.54
70.1	58.18	146.23	0.40	1.8360	0.0813	0.1999	0.0034	0.0725	0.0026	**0.0420**	**1.3013**	1058.43	29.09	1174.53	18.35	998.80	73.55	**1139.22**	15.34	-4.94
71.1	191.10	213.35	0.90	2.6927	0.0987	0.2409	0.0025	0.0829	0.0019	**0.0252**	**1.3045**	1326.45	27.15	1391.57	12.94	1267.14	44.95	**1379.09**	11.65	-4.37
72.1	119.06	171.01	0.70	2.0119	0.1056	0.2029	0.0041	0.0790	0.0028	**0.0393**	**1.4970**	1119.52	35.60	1190.61	22.23	1170.67	69.47	**1170.03**	18.84	-1.57
73.1	89.77	140.12	0.64	2.4721	0.1215	0.2244	0.0032	0.0819	0.0031	**0.0266**	**1.0358**	1263.90	35.54	1305.30	17.03	1242.66	74.68	**1297.51**	15.39	-2.08
74.1	18.99	132.59	0.14	1.8472	0.0802	0.1944	0.0025	0.0754	0.0022	**0.0317**	**1.1469**	1062.44	28.59	1145.02	13.72	1076.96	59.05	**1128.86**	12.32	-1.85
75.1	46.26	86.18	0.54	2.4977	0.1393	0.2466	0.0041	0.0822	0.0025	**0.0297**	**1.6456**	1271.37	40.45	1420.98	21.38	1249.22	59.83	**1384.52**	18.50	-4.96
76.1	42.46	99.97	0.42	2.8218	0.1360	0.2387	0.0039	0.0842	0.0026	**0.0288**	**1.5222**	1361.35	36.13	1379.74	20.38	1296.81	59.39	**1375.34**	17.89	-3.18
77.1	40.05	110.34	0.36	1.7959	0.0868	0.1786	0.0025	0.0711	0.0023	**0.0292**	**1.0797**	1043.96	31.52	1059.18	13.87	958.59	67.53	**1056.78**	12.80	-3.86
78.1	43.98	53.16	0.83	2.6365	0.1954	0.2422	0.0041	0.0834	0.0034	**0.0209**	**1.2084**	1310.88	54.56	1398.20	21.22	1276.73	79.15	**1385.99**	19.66	-4.27
79.1	11.06	26.20	0.42	2.5030	0.4845	0.2232	0.0054	0.0827	0.0042	**0.0112**	**1.2752**	1272.90	140.43	1299.01	28.51	1262.26	100.18	**1297.99**	27.97	-1.46
80.1	32.37	68.19	0.47	1.8456	0.1081	0.1845	0.0036	0.0721	0.0028	**0.0332**	**1.2895**	1061.86	38.56	1091.68	19.53	986.62	78.60	**1085.65**	17.55	-3.78
81.1	31.20	52.66	0.59	1.7774	0.1279	0.1911	0.0046	0.0647	0.0029	**0.0357**	**1.5775**	1037.23	46.76	1127.16	24.68	762.14	94.24	**1106.59**	21.71	-12.97
82.1	85.36	137.96	0.62	1.8291	0.0935	0.1877	0.0027	0.0741	0.0022	**0.0288**	**1.2478**	1055.96	33.57	1108.88	14.61	1044.19	58.72	**1100.33**	13.42	-2.03
83.1	83.47	143.66	0.58	1.9384	0.0834	0.1819	0.0028	0.0759	0.0024	**0.0341**	**1.1890**	1094.45	28.84	1077.50	15.53	1091.32	63.19	**1081.11**	13.91	0.37
84.1	67.31	200.44	0.34	1.8420	0.0672	0.1827	0.0020	0.0731	0.0020	**0.0305**	**1.0187**	1060.57	24.03	1081.90	11.16	1016.86	55.68	**1078.19**	10.20	-2.35

85.1	92.25	223.86	0.41	1.8029	0.0640	0.1829	0.0020	0.0702	0.0018	**0.0311**	**1.1332**	1046.52	23.19	1082.74	10.86	933.39	51.37	**1076.26**	9.88	-5.50
86.1	35.32	66.11	0.53	1.7499	0.1098	0.1678	0.0035	0.0746	0.0033	**0.0316**	**1.0523**	1027.11	40.54	999.73	19.18	1057.27	89.07	**1004.37**	17.63	1.96
87.1	79.94	144.90	0.55	1.7912	0.0738	0.1803	0.0024	0.0734	0.0023	**0.0329**	**1.0471**	1042.27	26.85	1068.76	13.24	1025.02	63.80	**1063.65**	11.97	-1.40
88.1	31.84	85.41	0.37	1.8842	0.0979	0.1933	0.0045	0.0692	0.0025	**0.0460**	**1.7676**	1075.54	34.48	1139.42	24.31	902.85	75.89	**1117.67**	19.93	-7.93
89.1	37.42	98.05	0.38	1.7862	0.1271	0.1811	0.0033	0.0759	0.0034	**0.0257**	**0.9705**	1040.45	46.32	1073.17	17.84	1091.76	88.89	**1069.00**	16.71	1.14
90.1	75.63	167.31	0.45	1.8726	0.0740	0.1825	0.0024	0.0752	0.0021	**0.0325**	**1.1663**	1071.44	26.17	1080.40	13.13	1073.18	55.17	**1078.66**	11.87	-0.20

Data within the acceptable concordia distance range (-3.5 to 4.6).